

1 **Title:**

2 Multi-channel intraneural vagus nerve recordings with a novel high-density carbon fiber
3 microelectrode array

4

5 **Authors:**

6 Ahmad A. Jiman^{1,2,3}, David C. Ratze^{2,4}, Elissa J. Welle^{1,2}, Paras R. Patel^{1,2}, Julianna M. Richie^{1,2},
7 Elizabeth C. Bottorff^{1,2}, John P. Seymour^{1,4,5}, Cynthia A. Chestek^{1,2,4}, Tim M. Bruns^{1,2}

8

9 1- Department of Biomedical Engineering, University of Michigan, Ann Arbor, MI, USA

10 2- Biointerfaces Institute, University of Michigan, Ann Arbor, MI, USA

11 3- Department of Electrical and Computer Engineering, King Abdulaziz University, Jeddah,

12 Saudi Arabia

13 4- Department of Electrical Engineering and Computer Science, University of Michigan, Ann

14 Arbor, MI, USA

15 5- Department of Neurosurgery, University of Texas Health Science Center, Houston, TX, USA

16

17 Corresponding Author:

18 Tim M. Bruns, Ph.D.

19 NCRC - B10 - A-169

20 2800 Plymouth Road

21 Ann Arbor, MI 48109, USA

22 Phone: (734) 647-8727

23 Email: bruns@umich.edu

24

25 **Abstract**

26 Autonomic nerves convey essential neural signals that regulate vital body functions. Recording
27 clearly distinctive physiological neural signals from autonomic nerves will help develop new
28 treatments for restoring regulatory functions. However, this is very challenging due to the small
29 nature of autonomic nerves. We developed a multi-channel, high-density, intraneural carbon fiber
30 microelectrode array (CFMA) for recording physiological action potentials from small autonomic
31 nerves. In this study, we inserted CFMA with up to 16 recording carbon fibers in the cervical vagus
32 nerve of 22 isoflurane-anesthetized rats. We recorded action potentials with signal-to-noise ratios
33 of 2.0-8.3 on multiple carbon fibers per experiment, determined conduction velocities of some
34 vagal signals in the afferent (0.7-1.0 m/sec) and efferent (0.7-8.8 m/sec) directions, and monitored
35 firing rate changes in breathing and blood glucose modulated conditions. Overall, these
36 experiments demonstrated that CFMAs are a novel interface for in-vivo intraneural action potential
37 recordings from autonomic nerves. This work is a milestone towards the comprehensive
38 understanding of physiological neural signaling and the development of innovative treatment
39 modalities for restoring vital functions controlled by autonomic nerves.

40

41

42 The autonomic nervous system has a major role in the regulation of unconscious functions that are
43 essential to the body. The system is divided into the sympathetic nervous system, which controls
44 “fight-or-flight” responses, and the parasympathetic nervous system, which regulates “rest-and-
45 digest” functions¹. A main parasympathetic nerve is the vagus nerve, which innervates many
46 visceral organs, such as the heart, lungs, stomach, liver, pancreas and intestines^{2,3}, and contributes
47 to the regulation of numerous autonomic functions, which include breathing, immune responses,
48 digestion, glucose metabolism and others⁴⁻⁸. The vagus nerve at the cervical level is partially
49 composed of myelinated A δ and B fibers^{9,10}, but the great majority of axons (over 80%) are
50 unmyelinated C-fibers^{2,11,12}. These fibers predominantly convey afferent (sensory) signals from
51 the innervated organs to the central nervous system¹³. Hence, the vagus nerve is an attractive target
52 for monitoring the physiological state of visceral organs for therapeutic or scientific objectives.

53 A class of therapies that has gained considerable interest in recent years is bioelectronic medicine,
54 which targets autonomic nerves to detect and alter neural activity for restoring autonomic
55 functions¹⁴⁻¹⁶. The variety of bioelectronic medicine applications that target the vagus nerve have
56 led to clinical trials on vagus nerve stimulation (VNS) for patients with epilepsy¹⁷, stroke¹⁸,
57 depression¹⁹, rheumatoid arthritis²⁰, obesity²¹, and type-2 diabetes²², among others. Despite the
58 therapeutic benefits of VNS and bioelectronic medicine, stimulation patterns are generally selected
59 by experimenting with different parameters without monitoring the physiological signaling in the
60 nerve. A key element that is needed to achieve the full potential of bioelectronic medicine is a
61 better understanding of neural signaling in normal and modulated physiological conditions.

62 Recording neural activity from autonomic nerves is very challenging due to the often sub-
63 millimeter nature of these nerves^{23,24}, the protective layers surrounding the nerve (epineurium),
64 bundle of axons (perineurium) and individual axons (endoneurium)^{25,26}, and the low-amplitude

65 waveforms generated from small unmyelinated C-fibers²⁷ that dominate autonomic nerves^{28,29}.
66 Studies have applied electrical stimulation on autonomic nerves to record evoked neural activity
67 using extraneural electrodes, which record from outside the nerve^{9,30}, and intraneural electrodes,
68 which penetrate the nerve³¹. Although electrical stimulation-evoked responses can be useful in
69 determining the type of activated fibers, these responses do not represent physiological neural
70 signaling. A few research groups have obtained physiological neural recordings from autonomic
71 nerves using extraneural cuff electrodes³²⁻³⁶. However, extraneural electrodes lack spatial
72 selectivity, as these electrodes record the compound activity of hundreds to thousands of axons
73 from outside the nerve. Intraneural electrodes penetrate the nerve to be closer to axons and provide
74 better selectivity and higher signal-to-noise ratio (SNR) recordings than extraneural electrodes^{25,26}.
75 Intraneural high-density Utah slanted electrode arrays (HD-USEAs) have 48 electrodes (30-100
76 μm tapered diameter) in a 5x10 configuration (pitch of 200 μm ; corner electrodes used as reference
77 and ground) and have been used to record signals in cat pudendal nerves, which have an
78 approximate diameter of 1 mm^{37,38}. This configuration of the silicon-based HD-USEA is large
79 (1x2 mm) and rigid for most autonomic nerves, which are often under 1 mm in diameter. For
80 recording from small-diameter (≤ 0.5 mm) autonomic nerves, carbon nanotube (CNT) electrodes
81 have demonstrated high SNR recordings (> 10 dB) in rat glossopharyngeal and vagus nerves
82 (diameter of 100-300 μm)²³. This was achieved by inserting two CNT electrodes (10 μm in
83 diameter) in a nerve target at a 2-mm separation to obtain a single differential recording. Another
84 research group inserted 4-channel carbon fiber arrays (electrode diameter ≤ 15 μm , pitch of 150
85 μm) in tracheosyringeal nerves of zebra finch birds, which are 125 μm in diameter and mostly
86 composed of myelinated fibers (99%)³¹. They obtained spontaneous recordings but primarily
87 demonstrated electrical stimulation-evoked compound neural responses. Autonomic nerves are

88 typically dominated by hundreds to thousands of unmyelinated fibers^{28,29,39,40}. The fibers of the
89 vagus nerve in particular innervate multiple critical organs and contribute to the regulation of many
90 autonomic functions²⁻⁸. Therefore, a need remains for an intraneural electrode array that can record
91 physiological single-neuron activity at multiple sampling locations within small autonomic nerves.

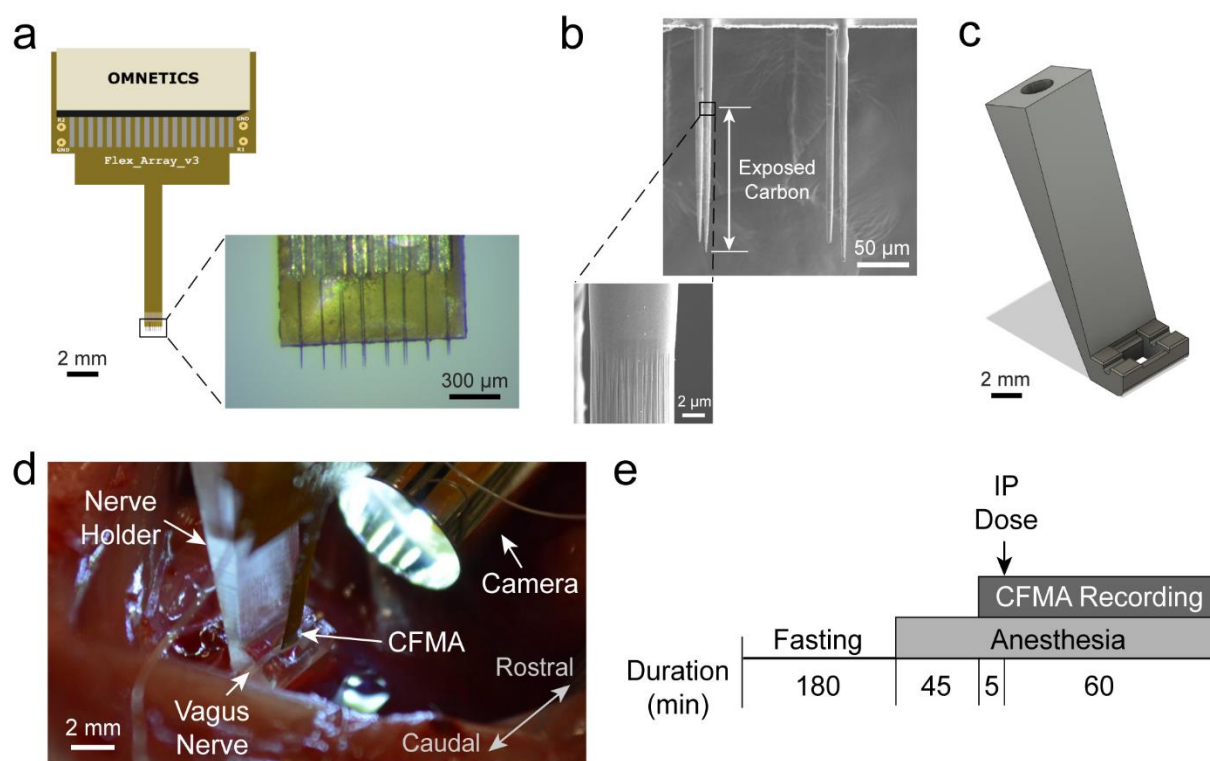
92 Our research group has developed a novel, multi-channel, blowtorch-sharpened, intraneural carbon
93 fiber microelectrode array (CFMA) for small autonomic nerves. The CFMA has ultra-small
94 recording electrodes (8-9 μm in diameter, 150-250 μm in length) in a higher-density configuration
95 than previously reported arrays (16 carbon fibers in 2 rows, with a 132 μm pitch along the array
96 and 50 μm between rows). Prior versions of the CFMA with longer (500-5000 μm), unsharpened
97 carbon fibers have demonstrated high SNR recordings with minimal tissue damage in the rat
98 cerebral cortex⁴¹⁻⁴⁴. We hypothesized that this novel CFMA would obtain physiological action
99 potential recordings with high SNR in small autonomic nerves. In this study, we inserted CFMAs
100 in rat cervical vagus nerves (diameter of 300-500 μm). We recorded action potentials on multiple
101 carbon fibers per experiment, determined the propagation direction and conduction velocity of
102 some vagal signals, and monitored changes in neural activity in breathing and blood glucose
103 modulated conditions.

104

105 **Results**

106 We fabricated CFMAs with 16 carbon fibers in a 2x8 configuration. Fibers within each row had a
107 pitch of 132 μm , and the two rows were separated by 50 μm (Figure 1a). The carbon fibers, which
108 had a diameter of 8-9 μm , were cut to 150-250 μm in length and the tips were sharpened with a
109 blowtorch (Figure 1b). The active recording site for a carbon fiber is coated with poly(3,4-

110 ethylene-dioxythiophene):sodium p-toluenesulfonate (PEDOT:pTS) and spans 135-160 μm in
111 length from the tip. To facilitate CFMA insertion in a rat vagus nerve, we designed a nerve-holder
112 to secure and elevate the vagus nerve away from fluid and breathing motions of the cervical cavity,
113 and allow accurate positioning of a small camera to visualize the CFMA-nerve interface during
114 insertion (Figure 1c).



115
116 **Figure 1. Carbon Fiber Microelectrode Array (CFMA) and experimental setup.** (a) CFMA with 16 blowtorch-
117 sharpened carbon fibers in a 2x8 configuration. (b) Scanning Electron Microscopy (SEM) images of sharpened
118 carbon fibers. Arrows indicate an exposed (non-insulated) carbon fiber region with a length of $\sim 140 \mu\text{m}$ from the
119 tip. (c) Design of a nerve-holder to facilitate CFMA insertion in a rat vagus nerve. Dimensions of the design are
120 shown in Supplementary Figure 1. (d) Surgical setup for inserting CFMA in the vagus nerve. (e) Timeline for the
121 experimental protocol. An intraperitoneal (IP) dose of glucose, insulin, 2-deoxy-D-glucose, or saline was injected to
122 modulate blood glucose concentration levels.

123
124 We inserted 6 CFMAs in the left cervical vagus nerve of 22 Sprague-Dawley rats. We observed
125 neural activity on 167 out of 326 inserted functional carbon fibers (impedance $< 1 \text{ M}\Omega$). The neural

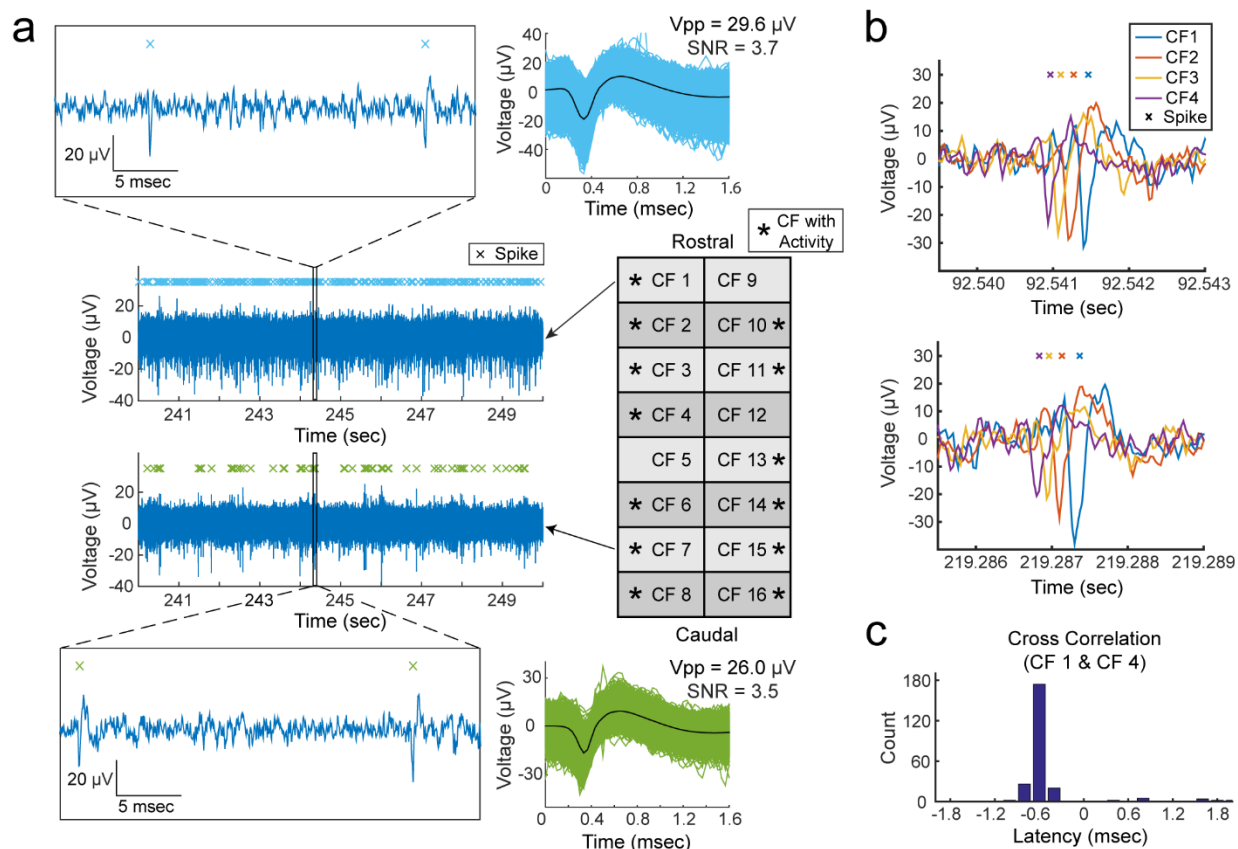
126 activity on each carbon fiber was sorted into 1 neural cluster (n=160) or 2 neural clusters (n=7).
127 The functional carbon fibers had an average impedance of 31.3 ± 42.0 k Ω (mean \pm standard
128 deviation) in saline before an experiment, 70.8 ± 81.9 k Ω in the nerve immediately after insertion,
129 and 94.7 ± 146.7 k Ω in the nerve at the end of the experiment. Three of the CFMAs were used in
130 more than one experiment (4-8 experiments per CFMA), which initially had a total of 48 functional
131 carbon fibers (16 carbon fibers per CFMA) with an average impedance of 52.8 ± 36.8 k Ω after
132 insertion in the first experiment. After insertion in the fourth experiment, 45 carbon fibers on these
133 three CFMAs (14-16 carbon fibers per CFMA) remained functional with an average impedance of
134 92.6 ± 149.5 k Ω . On average for a single experiment, we made 2.3 ± 2.9 attempts to insert a CFMA
135 with 14.8 ± 1.8 functional carbon fibers and observed neural activity on 7.6 ± 5.8 carbon fibers.
136 There were no distinctive differences among the recordings of rats with different gender or sizes.

137 *Multi-Channel Recordings of Vagal Nerve Activity*

138 We observed physiological neural activity in the vagus nerve on at least one recording carbon fiber
139 in 19 of the total 22 experiments. The recorded neural activity was sorted into clusters and the
140 mean peak-to-peak amplitudes of the sorted clusters were between 15.1 and 91.7 μ V with SNR of
141 2.0-8.3. An example of vagal nerve activity on multiple recording carbon fibers from the same
142 experiment is shown in Figure 2a.

143 Propagation of vagal signals were detected along adjacent recording carbon fibers in some
144 experiments. We observed neural signals in 10 experiments propagating in the afferent direction
145 with conduction velocities of 0.7-1.0 m/sec over the span of 2-7 carbon fibers (132-792 μ m).
146 Furthermore, we monitored efferent signals conducting at 0.7-8.8 m/sec along 2-5 carbon fibers
147 (132-528 μ m) in 5 experiments. Examples of propagating afferent signals are shown in Figure 2b

148 with cross-correlation to inspect the latency of those signals along CFMA carbon fibers (Figure
149 2c).



150
151 **Figure 2. Representative recordings of physiological vagal nerve activity and signal propagation along CFMA**
152 **carbon fibers (CFs).** (a) Recordings of vagal nerve activity on 2 carbon fibers (CF 1 and CF 7) in the same
153 experiment showing distinctive signals. The firing of sorted spikes (marked with x) are unique across CFs. (b)
154 Instances of signal propagation along CF 1 – CF 4. (c) Cross correlation of spikes on CF 1 and CF 4. The prevalent
155 latency occurred at -0.6 msec with a count of 174 spikes (55.8% of spikes on CF 4). At latency of -0.6 msec, the
156 spikes occurred on CF 4 before CF 1, suggesting that the signal is propagating in the afferent direction at a
157 conduction velocity of 0.7 m/sec.

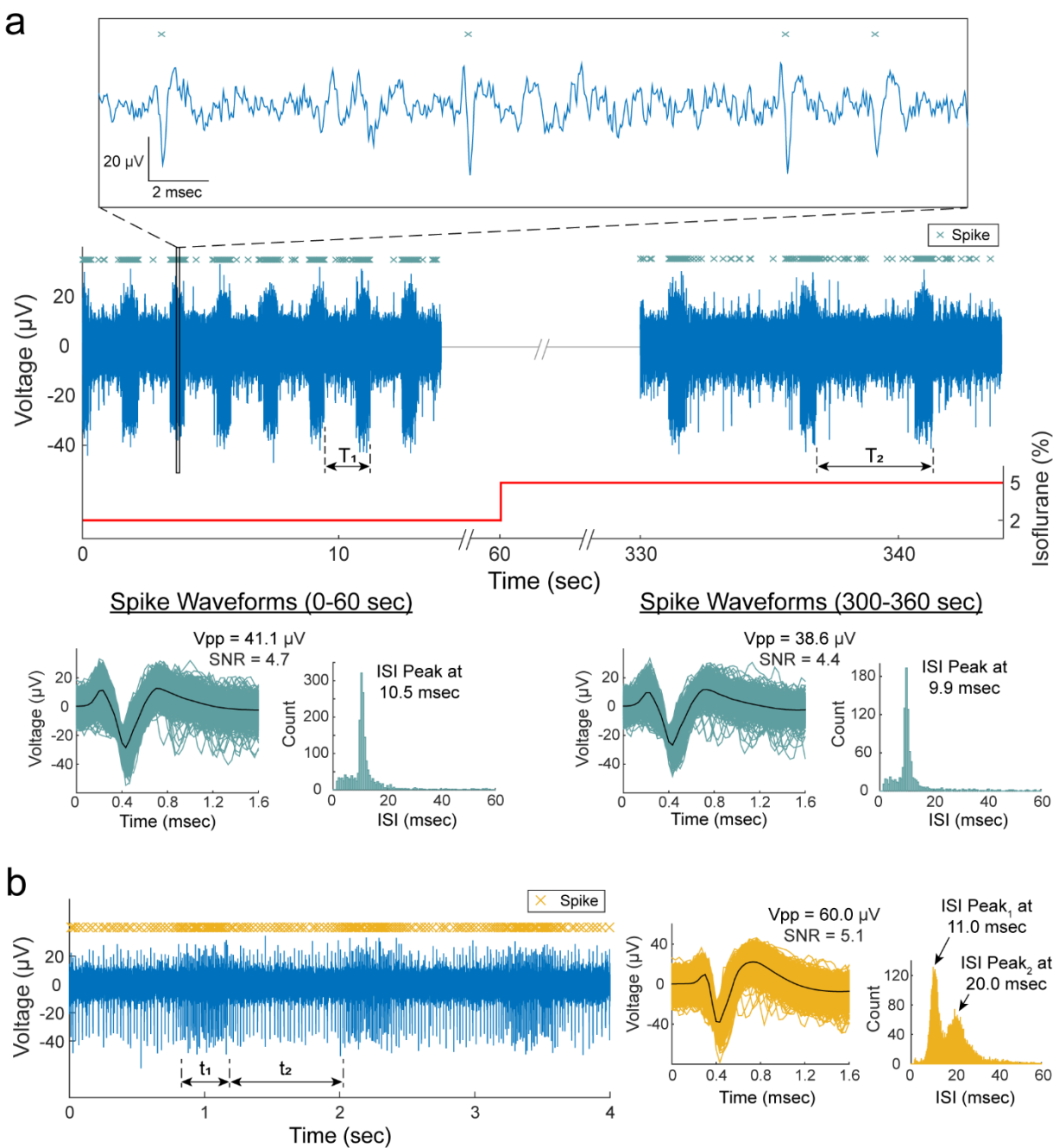
158
159 **Breathing-Related Neural Activity**

160 We observed vagal signals with periodic bursting firing behavior (n=6 experiments) at repetition
161 rates of 39.4 ± 10.8 cycles/min, which were similar to the animals' breathing rates of 39.3 ± 9.9
162 breaths/min (Figure 3). In a subset of experiments (n=3), we reduced the breathing rate to $20.0 \pm$

163 8.0 breaths/min by increasing the depth of anesthesia, and the firing-burst repetition rates reduced
164 to a similar level at 19.1 ± 10.3 cycles/min, with maintained peak-to-peak amplitudes (31.7 ± 11.6
165 μV to $29.3 \pm 10.1 \mu\text{V}$) and inter-spike interval (ISI) peak values (9.2 ± 1.6 msec to 10.5 ± 1.6
166 msec), as shown in the example in Figure 3a. The periodic bursting behaviors were usually firing
167 at one ISI peak of 9.5 ± 1.3 msec. However, in two experiments, two distinct ISI peaks were
168 observed at 9.8 ± 1.8 msec and 24.2 ± 6.0 msec (e.g. Figure 3b).

169

170

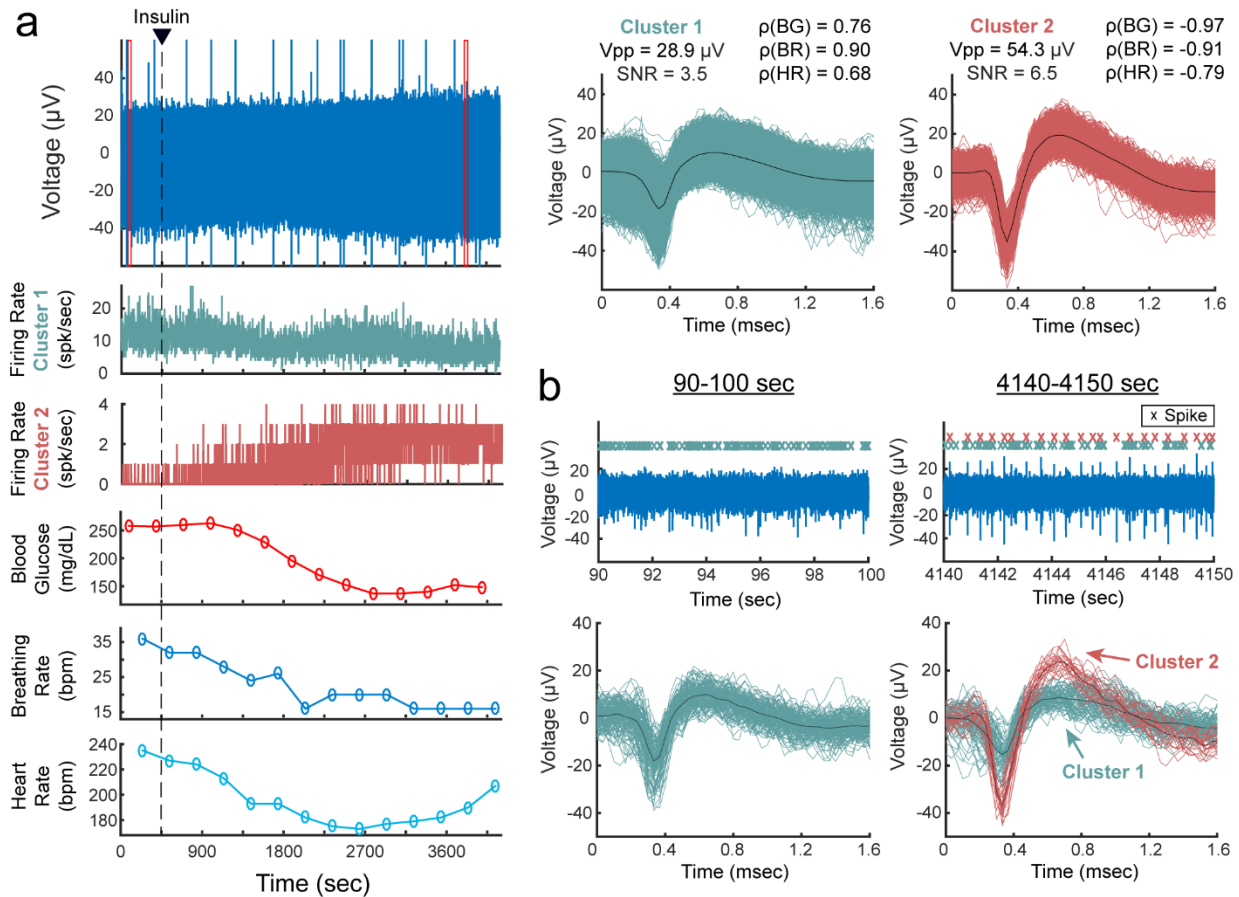


171

172 **Figure 3. Breathing-related neural activity.** (a) Recordings of vagus nerve activity at 2% and 5% isoflurane. The
 173 bursting firing behavior had a repetition rate of 32.2 cycles/min ($1/T_1$) during animal's breathing rate of 32
 174 breaths/min at 2% isoflurane. The firing-behavior repetition rate reduced to 14.2 cycles/min ($1/T_2$) as the breathing
 175 rate reduced to ~12 breaths/min at 5% isoflurane. The average peak-to-peak amplitude (V_{pp}) and inter-spike
 176 interval (ISI) peaks were similar for the spike waveforms at 2% and 5% isoflurane. (b) Bursting firing behavior at
 177 two distinct ISIs indicated at the t_1 and t_2 durations. The animal's breathing rate was ~44 breaths/min and the
 178 repetition rate for the bursting firing behavior was 47.3 cycles/min ($1/[t_1+t_2]$).

179 *Neural Firing Rate Behavior in Blood Glucose Modulation Conditions*

180 In each experiment, we recorded vagal nerve activity for a baseline period of at least 5 minutes
181 before the intraperitoneal (IP) injection of a blood glucose modulation dose (glucose, insulin, 2-
182 deoxy-D-glucose, or saline). Recordings were continued for 60 minutes after the injection.
183 Physiological parameters (blood glucose concentration, breathing rate, and heart rate) were
184 measured every 5 minutes throughout the entire experiment. The recorded neural activity were
185 sorted into 174 clusters. The firing rate of these clusters showed moderate or high correlation
186 coefficients ($|\rho| \geq 0.3$) with one (n=15), two (n=35), or all three (n=96) of the tracked physiological
187 parameters. However, correlation coefficients did not show clear associations between any glucose
188 modulation dosing and any of the physiological parameters across experiments. An experiment
189 with a carbon fiber that recorded the activity of 2 sorted clusters, along with the physiological
190 measurements (blood glucose concentration, breathing rate and heart rate) and correlation
191 coefficients, is shown in Figure 4.



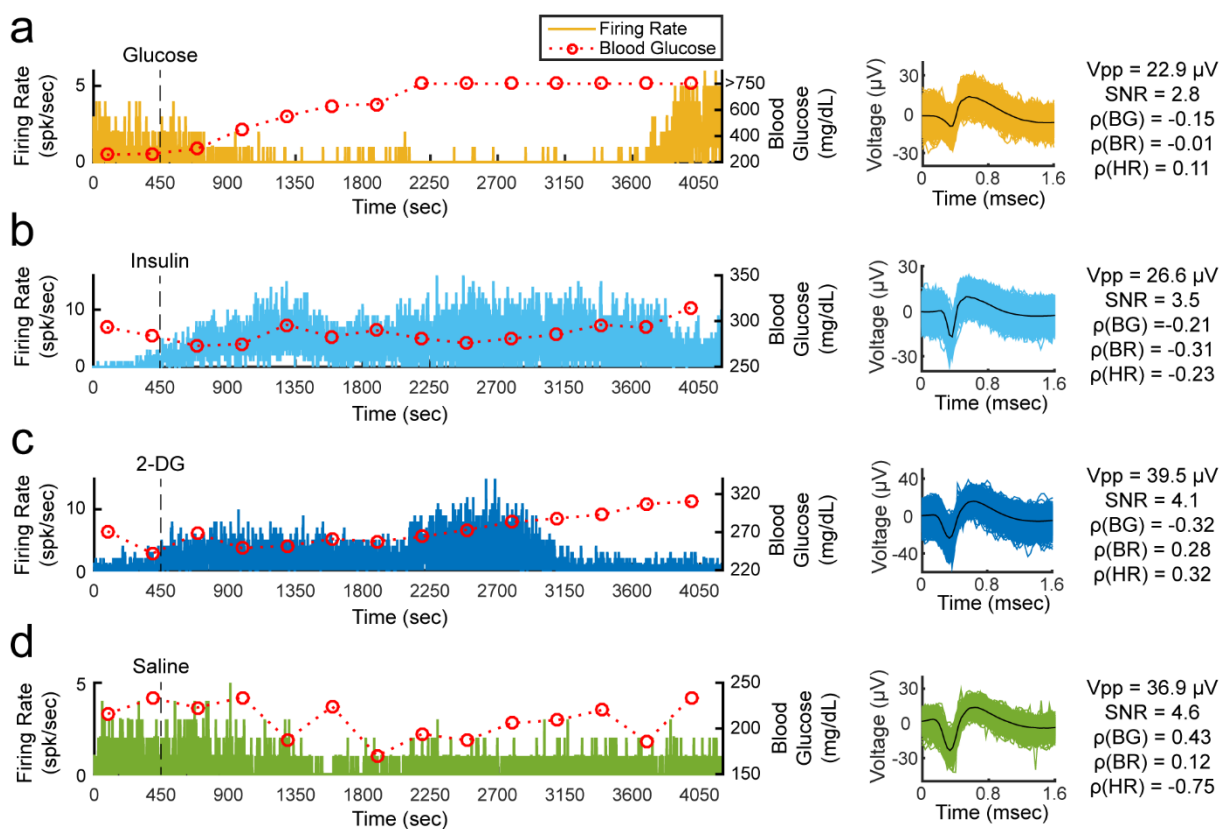
192

193 **Figure 4. Vagus nerve recordings with sorted clusters in an insulin-injected experiment.** (a) Filtered signal of a
 194 vagus nerve recording, firing rates of the two sorted clusters, and measurements of blood glucose (BG)
 195 concentration, breathing rate (BR) and heart rate (HR). The waveforms of the sorted clusters are shown with the
 196 average peak-to-peak amplitude (Vpp), signal-to-noise ratio (SNR), and correlation coefficients (ρ) between cluster
 197 firing rate and BG, BR and HR measurements. The red boxes in the voltage plot indicate the time-window for the
 198 plots in b. (b) Filtered signal of the vagus nerve recording before and after insulin injection, and the spike
 199 waveforms of the two sorted clusters within each 10-sec window.

200

201 Although correlation coefficients did not show a clear relationship between any of the glucose
 202 modulation doses and physiological parameters, we observed clusters with interesting firing rate
 203 behaviors after injection of a modulation dose, as shown in Figure 5. In some glucose injection
 204 experiments (n=4), we observed neural clusters (n=11) with an average peak-to-peak amplitude of
 205 $24.7 \pm 6.4 \mu\text{V}$ with an initial firing rate of 6.8 ± 8.9 spikes/sec that decreased after administration

206 of glucose to 1.8 ± 2.4 spikes/sec (e.g. Figure 5a). In some experiments with an insulin injection
207 (n=4), neural clusters (n=4) with amplitudes of 53.3 ± 28.0 μV peak-to-peak increased their firing
208 rates from 1.2 ± 1.8 spikes/sec to 7.6 ± 10.4 spikes/sec at 1-13 minutes after insulin administration
209 (e.g. Figure 5b). Injection of 2-deoxy-D-glucose (2-DG) induced a similar neural response to
210 insulin in some experiments (n=2). Starting at 1-9 minutes after 2-DG administration, clusters
211 (n=6) with an average amplitude of 29.2 ± 8.1 μV peak-to-peak increased their firing rates from
212 3.8 ± 4.6 spikes/sec to 9.8 ± 10.1 spikes/sec (e.g. Figure 5c). A summary of all the performed
213 experiments is shown in Supplementary Table 1.



214

215 **Figure 5. Examples of sorted clusters and their firing rates in blood glucose modulated conditions.** The
216 clusters were observed in blood glucose modulation experiments with an intraperitoneal (IP) injection of (a)
217 glucose, (b) insulin, (c) 2-deoxy-D-glucose (2-DG), or (d) saline. The waveforms of the sorted clusters are shown
218 with the average peak-to-peak amplitude (V_{pp}), signal-to-noise ratio (SNR), correlation coefficients (ρ) between
219 cluster firing rate and blood glucose (BG) concentration, breathing rate (BR) and heart rate (HR). Blood glucose
220 concentration measurements above 750 mg/dL were not available due to the limitations of the glucometer.

221 **Discussion**

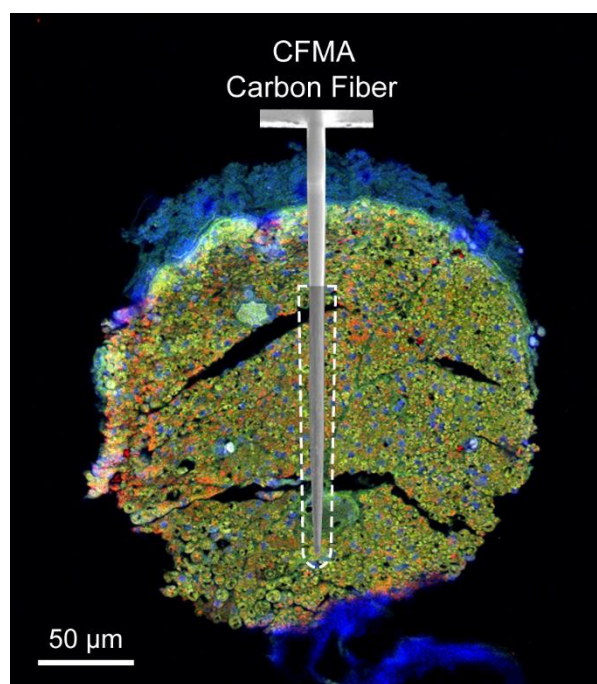
222 We developed a multi-channel, high-density, intraneural carbon fiber microelectrode array
223 (CFMA) for recording neural signals in autonomic nerves (Figure 1). Using the CFMA, we
224 obtained axonal action potential recordings in rat cervical vagus nerves with signal-to-noise ratio
225 (SNR) of 2.0-8.3. We recorded physiological vagal nerve activity that was unique across multiple
226 channels per experiment (Figure 2a), determined the propagation direction and conduction velocity
227 of some vagal signals (Figure 2b), and monitored changes in neural activity in physiologically
228 modulated conditions (Figures 3-5). These data demonstrate CFMA as a new interface for in-vivo
229 intraneural recordings. This work, to our knowledge, is the first to demonstrate in-vivo
230 physiological action potential recordings on multiple channels in a sub-millimeter autonomic
231 nerve. Monitoring physiological signaling in autonomic nerves will help researchers better
232 understand the neural control and feedback processes for autonomic organs, which is a key element
233 for developing innovative treatment modalities to restore vital body functions regulated by
234 autonomic nerves.

235 Our experimental recordings demonstrated CFMA as a multi-channel, intraneural array for small-
236 diameter (≤ 0.5 mm) autonomic nerves. In prior work, the high-density Utah slanted electrode
237 array (HD-USEA) was implanted in a 1-mm diameter cat pudendal nerve³⁷. While the 48-channel,
238 200 μm pitch HD-USEA (footprint over 1 mm^2) was used to record physiological signaling from
239 autonomic organs (feline lower urinary tract)³⁷, the size of the HD-USEA electrode shanks (300-
240 800 μm in length, 30-100 μm in diameter)³⁸ are much larger than in the CFMA and would make
241 intraneural recordings in small autonomic nerves challenging. In our study, 16-channel CFMAs
242 (footprint less than 0.05 mm^2 ; 132 μm pitch along the array and 50 μm between two rows) with
243 ultra-small electrodes (150-250 μm in length, 8-9 μm in diameter) were implanted in small-

244 diameter (300-500 μm) rat vagus nerves. Another intraneural electrode that obtained physiological
245 recordings in small-diameter (100-300 μm) autonomic nerves (rat glossopharyngeal and vagus
246 nerves) are carbon nanotube (CNT) electrodes²³. Two single-channel CNT electrodes were
247 inserted with a 2-mm separation in a nerve target to obtain only a single differential recording in
248 that study. The CFMA recorded physiological neural activity on multiple channels (up to 16
249 channels), which allowed us to detect the propagation direction and conduction velocity of some
250 signals (Figure 2). The recording exposure site on each carbon fiber spans 135-160 μm in length
251 from the tip, which provided better spatial selectivity recordings than CNT electrodes that had an
252 exposed recording segment of ~ 500 μm . Another research group developed an intraneural 4-
253 channel carbon fiber array with a similar pitch (150 μm) as the CFMA but with longer carbon
254 fibers (≥ 350 μm) that recorded from tracheosyringeal nerves of zebra finch birds (diameter of 125
255 μm)³¹. They demonstrated an innovative blowtorching technique for sharpening carbon fibers to
256 directly insert carbon fibers in a nerve, which we adapted to our shorter (150-250 μm) CFMA
257 carbon fibers. Although an example of spontaneous activity was shown using the 4-channel array,
258 the majority of their demonstrated signals were evoked responses from electrical stimulation.

259 The observed spike waveforms in CFMA recordings from the vagus nerve (e.g. Figures 2-5) are
260 action potentials generated by individual neurons, based on the waveform shape and time scale (1-
261 2 msec)^{45,46}. Furthermore, we observed propagation of signals in the afferent and efferent direction
262 within the conduction velocity range for myelinated (A δ and B) and unmyelinated (C) fibers
263 (Figure 2), which are present in the vagus nerve^{9,10}. However, due to the similarity in the waveform
264 shapes and the normal variations in waveform amplitudes, we were not able to sort the detected
265 action potentials into clear single units per channel, with only a few channels yielding more than
266 one sortable cluster. The active recording site for a CFMA carbon fiber spans 135-160 μm in length

267 from the tip (Figure 1), which exposes the recording site to an estimation of over 200 axons within
268 a distance of 5 μm from the recording site (Figure 6). This estimation is based on the approximate
269 axon density in the rat vagus nerve, which has around 11,000 axons^{28,29} contained within a
270 diameter of about 300 μm . Further work on reducing the exposed recording site area may assist in
271 monitoring more localized axon activity with a lower background noise level^{24,42,44}. Moreover,
272 current spike-sorting algorithms are mostly designed for central nervous system recordings⁴⁷,
273 which assume the waveforms are from neuron cell bodies that generate higher amplitude
274 waveforms and have more diverse shapes than unmyelinated axons. Future work is needed to study
275 the recording nature in autonomic nerves and develop spike-sorting algorithms for axonal
276 recordings.



277
278 **Figure 6. Immunohistochemistry image of a rat cervical vagus nerve with a diagram of an inserted CFMA**
279 **carbon fiber.** The shaded region on the CFMA carbon fiber is the active recording site. The dashed lines specify an
280 area within a distance of 5 μm from the active recording site of one carbon fiber. The area is estimated to be
281 occupied by over 200 axons based on the typical axon density of a rat vagus nerve (~11,000 axons in 300 μm
282 diameter nerve)^{28,29}. The nerve sample in this image was stained with 4', 6-diamino-2-phenylindole (DAPI), myelin
283 basic protein (MBP), and anti-beta III tubuline (TUJ1) to show nucleotides (blue), myelin (green) and axons (red),
284 respectively.

285 Sorted clusters from our recorded vagal nerve activity showed interesting firing rate behavior that
286 may be related to the measured physiological parameters of breathing rate, heart rate and blood
287 glucose concentrations. We observed neural clusters with periodic firing-burst behavior at
288 repetition rates similar to the measured breathing rates (Figure 3). Vagus nerve fibers innervate the
289 lungs, with critical relevance for breathing control^{4,48,49}. Our observed vagal signals may be related
290 to the neural control over breathing or an afferent response to chest and/or lung expansion⁴⁸. We
291 also observed interesting changes in vagal firing rate behavior after injection of blood glucose
292 modulation doses (Figure 5). These experiments were performed on fasted rats, and neural signals
293 before the dose injection may represent vagal afferent signals to drive an increase in glucose intake.
294 The firing rate of clusters decreased after administration of glucose (e.g. Figure 5a), which may
295 suggest that the signaling for glucose intake was met. This observation aligns with previous studies
296 that showed neural recordings from dissected fibers of afferent hepatic vagus nerve branches in
297 isolated and perfused livers using wire electrodes⁵⁰, and compound neural activity from the
298 cervical vagus nerve using cuff electrodes after removing the nerve sheath³⁶. Both studies
299 demonstrated similar firing rate changes following the administration of glucose. The increase in
300 firing rate observed after insulin or 2-deoxy-D-glucose (2-DG) injection, which induces insulin-
301 like symptoms, may represent a surge of afferent activity to enhance the request for glucose intake
302 (e.g. Figure 5b,c), which aligns with the previously mentioned studies that also showed increased
303 afferent activity in the hepatic branch of vagus nerves using wire electrodes⁵⁰, and increased
304 compound activity of cervical vagus nerves using cuff electrodes³⁶ within 10 minutes after
305 administration of insulin or 2-DG. However, these observed responses were inconsistent across
306 our experiments with identical injection doses, which may be due to variations in CMFA sampling
307 of neural activity within the nerve. Moreover, there were similarities in the blood glucose

308 concentration trends during an experiment to the other measured physiological parameters (i.e.
309 breathing rate and heart rate) in most experiments (e.g. Figures 4 and 5). The anesthetic agent we
310 used in our experiments was isoflurane, which maintained consistent and stable depth of anesthesia
311 for recording vagal nerve activity with ultra-small carbon fibers. In preliminary experiments using
312 other agents (e.g. ketamine), occasional muscle twitches would lead to CFMA movement or
313 carbon fiber breakage, which were not observed under isoflurane. However, isoflurane anesthesia
314 suppresses neural activity in the central and autonomic nervous systems and impacts multiple
315 physiological parameters, including blood glucose concentration, respiration, and arterial
316 pressure^{51,52}. Although this work showed unique in-vivo action potential recordings from the vagus
317 nerve using CFMA, experiments with minimal or no anesthesia would allow more physiological
318 activities to occur and may be necessary to clearly link vagal nerve activity to physiological
319 changes.

320 This work had numerous limitations. The exact insertion location for the CFMA arrays in the vagus
321 nerve varied between our experiments. The rat cervical vagus nerve is estimated to contain around
322 11,000 axons^{28,29} that regulate many autonomic functions⁴. To illustrate this variation, potential
323 breathing-related signals (e.g. Figure 3) were only observed in 6 out of the 22 experiments,
324 although all the rats were breathing normally during the experiments. Furthermore, we detected
325 propagation direction of some, but not all, recorded vagal signals (e.g. Figure 2), likely due to the
326 variation in CFMA insertion alignment along the nerve. Additional work on redesigning the
327 electrode configuration may be needed to cover a wider range of axonal activity while providing
328 high selectivity for individual recording sites, such as with staggered rows of carbon fibers with
329 variable lengths. Another limitation is the requirement to lift the nerve for CFMA insertion, which
330 applies tension on the nerve due to the nerve-holder design. Although the nerve-holder added the

331 risk of nerve injury, the nerve-holder was necessary to position a camera to visualize the alignment
332 of CFMA carbon fibers with the vagus nerve for insertion (Figure 1). Redesigning the nerve-holder
333 and possibly restructuring the implantation procedure may be needed to eliminate the applied
334 tension and avoid the risk of injuring the nerve. This study only demonstrated CFMA recordings
335 from the rat vagus nerve. However, the CFMA also recorded action potentials from the cat
336 pudendal nerve and rat sural nerve, a branch of the sciatic nerve, in preliminary experiments (data
337 not shown). Future studies on physiological neural recordings from various peripheral nerves will
338 provide new perspectives on neural control processes.

339 Overall, our experiments demonstrated that CFMAs are a novel interface for in-vivo, high-density,
340 multi-channel, intraneural action potential recordings in small autonomic nerves. Further work is
341 needed to refine the selectivity of CFMA and develop a chronic form for long-term, behavioral
342 recordings in autonomic nerves without the presence of anesthesia. This work provided insights in
343 intraneural axonal recordings and is a milestone towards the comprehensive understanding of
344 physiological signaling in autonomic nerves, which may lead to the development of innovative
345 treatment modalities for restoring regulatory functions.

346

347 **Methods**

348 *Fabrication of Carbon Fiber Microelectrode Array*

349 The independent components for fabricating carbon fiber microelectrode arrays (CFMAs) are
350 described in detail elsewhere^{42–44,53}. Briefly, a printed circuit board (PCB) was custom
351 manufactured (MicroConnex, Snoqualmie, WA, USA). A connector (A79024-001, Omnetics

352 Connector Corp., Minneapolis, MN, USA) was soldered on one end of the PCB and covered with
353 epoxy. On the other end, 16 bare carbon fibers (T-650/35 3 K, Cytec Industries, Woodland Park,
354 NJ, USA) with a length of 2-3 mm were attached to the PCB in a 2-row (2x8) configuration. The
355 pitch was 132 μm within a row and the separation between the two rows was 50 μm . The array
356 was coated with approximately 800 nm of parylene-c (PDS 2035, Specialty Coating Systems Inc.,
357 Indianapolis, IN, USA) for insulation. The insulated carbon fibers had a diameter of 8-9 μm and
358 were cut down to 150-250 μm in length. The base of the carbon fibers were submerged in water
359 and the tips were sharpened with a blowtorch³¹ (MT-51, Master Appliance Corp., Racine, WI,
360 USA) after aligning the carbon fibers with their reflection on the underside of the water surface.
361 The exposed carbon on the sharpened tips (135-160 μm) were electrodeposited with poly(3,4-
362 ethylene-dioxythiophene):sodium p-toluenesulfonate (PEDOT:pTS) by applying 600 pA/fiber for
363 600 sec. Finally, individual ground and reference wires (AGT05100, World Precision Instruments,
364 Sarasota, FL, USA) were soldered to the PCB.

365 *Design of Nerve-Holder*

366 To facilitate the insertion of a CFMA in a vagus nerve, we designed a nerve-holder to secure and
367 elevate the vagus nerve away from fluid and breathing motions of the cervical cavity, and allow
368 accurate positioning of a small camera to visualize the CFMA-nerve interface during insertion.
369 The nerve-holder had a hollow center to allow insertion of carbon fibers without breakage, and to
370 drain excess fluid around the nerve which may obscure the camera view. To handle the nerve-
371 holder, a circular threaded rod (21YN67, Grainger Inc., Lake Forest, IL, USA) was inserted in the
372 holder and was connected to a soldering arm (900-015, Eclipse, Amelia Court House, VA, USA).
373 The nerve-holder was designed using a computer-aided design (CAD) software (Fusion 360,

374 Autodesk, San Rafael, CA, USA) and 3D-printed with clear resin (Form 2, Formlabs, Somerville,
375 MA, USA). The dimensions of the design are shown in Supplementary Figure 1.

376 *Animal Surgery*

377 All experimental procedures were approved by the University of Michigan Institutional Animal
378 Care and Use Committee (IACUC). Non-survival experiments were performed on male (0.48-0.83
379 kg) and female (0.36-0.42 kg) Sprague-Dawley rats (Charles Rivers Laboratories, Wilmington,
380 MA, USA). The animals were housed in ventilated cages under controlled temperature, humidity,
381 and photoperiod (12-h light/dark cycle), and provided with laboratory chow (5L0D, LabDiet, St.
382 Louis, MO, USA) and tap water ad libitum. The rats were fasted for 3 hours before the procedure.
383 Anesthesia was induced by 5% isoflurane (Fluriso, VetOne, Boise, ID, USA) and maintained at 2-
384 3% isoflurane. Rats were placed on a heating pad (ReptiTherm, Zoo Med Laboratories Inc., San
385 Luis Obispo, CA, USA). A vitals-monitor (SurgiVet, Smiths Medical, Norwell, MA, USA) was
386 used to monitor heart rate with an oxygen saturation (SpO₂) sensor. A midline ventral cervical
387 incision was made, and retractors (17009-07, Fine Science Tools Inc., Foster City, CA, USA) were
388 used to maintain the cervical opening. Using a dissection microscope (Lynx EVO, Vision
389 Engineering Inc., New Milford, CT, USA), the left cervical vagus nerve (9-12 mm in length) was
390 isolated from the carotid artery and surrounding tissue using fine forceps (00632-11, Fine Science
391 Tools Inc., Foster City, CA, USA). The vagus nerve was lifted (~2 mm) and placed on the nerve-
392 holder to facilitate CFMA insertion. The heating pad and dissection microscope were disconnected
393 to reduce electrical noise.

394

395

396 ***CFMA Insertion***

397 The CFMA was accurately controlled by a micromanipulator (KITE-R, World Precision
398 Instruments, Sarasota, FL, USA) that was secured on an optical breadboard (MB1218, Thorlabs
399 Inc., Newton, NJ, USA) under the animal. The ground wire for the CFMA was inserted
400 subcutaneously in the cervical region and the reference wire was placed in fluid or tissue
401 underneath the nerve-holder. A small pen-shaped camera (MS100, Teslong, Shenzhen, China) was
402 placed in the cervical opening to visualize and align the CFMA fibers for insertion. The nerve was
403 rinsed with saline (0.9% NaCl, Baxter International Inc., Deerfield, IL, USA) and the CFMA was
404 inserted in the vagus nerve.

405 The CFMA was connected to a neural interface processor (Grapevine, Ripple LLC, Salt Lake City,
406 UT, USA) that recorded signals at a sampling rate of 30 kHz on a linked desktop computer.
407 Impedances were measured with the neural interface processor at 1 kHz in saline before the
408 procedure, in the nerve immediately after insertion, and in the nerve at the end of the experiment.

409 ***Experimental Protocol***

410 After completion of surgery and insertion of the CFMA, a baseline recording period of at least 5
411 minutes was obtained. A dose of glucose (n=6; 1 g, Dextrose 50%, Hospira, Lake Forest, IL, USA),
412 insulin (n=6; 20 U, Vetsulin, Merck Animal Health, Madison, NJ, USA), 2-deoxy-D-glucose (n=6;
413 60 mg, D8375-1G, Sigma-Aldrich, St. Louis, MO, USA), or saline (n=4; 1.0 mL, 0.9% NaCl,
414 Baxter International Inc., Deerfield, IL, USA) was injected intraperitoneally (IP). Recordings from
415 the CFMA were continued for 60 minutes after the injection. Measurements of blood glucose
416 concentration with a glucometer (AlphaTRAK 2, Abbott, Abbott Park, IL, USA), heart rate with
417 the SpO₂ sensor, and breathing rate with a timer were obtained every 5 minutes. The glucometer

418 was unable to measure blood glucose concentrations above 750 mg/dL in one experiment due to
419 the limitations of the glucometer. In experiments with observed breathing-related neural signals
420 (n=3), a recording period of 1 minute was obtained at 2% isoflurane, followed by a 5-minute
421 recording at 5% isoflurane. At the end of the experiment, animals were euthanized with an
422 overdose of sodium pentobarbital (400 mg/kg IP, Euthanasia Solution, VetOne, Boise, ID, USA).

423 *Analysis of Neural Recordings*

424 The recorded signals were sorted into clusters using Wave_clus⁵⁴, which is a spike-sorting
425 MATLAB-based algorithm that uses wavelet decomposition to extract waveform features and
426 superparamagnetic clustering to cluster the spikes. The signals were filtered with a band-pass filter
427 at 300-10,000 Hz. The spike detection threshold was set between 3.3 and 10.1σ [$\sigma = \text{median}(|\text{filtered signal}| / 0.6745)$]⁵⁴. The sorted clusters were exported to MATLAB (R2014b, MathWorks,
428 Natick, MA, USA) for analysis. Firing rates were calculated with a bin duration of 1 sec. To
429 calculate signal-to-noise ratio (SNR), the mean peak-to-peak amplitude (Vpp) of a sorted cluster
430 was determined and noise intervals with a total duration of at least 7 sec were specified at periods
431 with no occurring spikes or artifacts [$\text{SNR} = \text{Vpp} / (2 \times \text{standard deviation of noise})$]^{41,43}. Cross-
432 correlation was performed between the sorted clusters across all the recording carbon fibers of a
433 CFMA to inspect the latency of spikes along the CFMA. Latencies with high occurrences (count
434 \gg mean occurrence) were identified, and the signal traces on adjacent recording carbon fibers
435 were manually reviewed to confirm instances of signal propagation before determining the
436 conduction velocity and signal propagation direction for these high-occurring latencies. The bin-
437 size for the latency counts was set at 0.2 msec, except for one experiment that had multiple high
438 counts at zero latency with this 0.2 msec bin-size resolution. For this experiment only, the bin-size
439 was set at 0.01 msec to provide latency counts with higher resolution. The correlation coefficient
440

441 (ρ) was calculated for all sorted clusters between the firing rate of each cluster and the measured
442 physiological parameters (breathing rate, heart rate and blood glucose concentration) for that
443 experiment. Since the physiological measurements were much less frequent (every 5 minutes) than
444 cluster firing rates (every second), the average cluster firing rate for 1 minute, centered at the time
445 of each physiological measurement, was determined and used for the correlation coefficient
446 computations. When appropriate, data are presented as mean \pm standard deviation (SD).

447 ***Data Availability***

448 All raw recordings, sorted neural clusters, and analysis codes will be available on the Blackfynn
449 data repository platform at DOI: <https://doi.org/10.26275/j5wc-rwcr> once it has completed NIH
450 SPARC data curation.

451

452 **References**

- 453 1. McCorry, L. K. Physiology of the Autonomic Nervous System. *Am. J. Pharm. Educ.* **71**,
454 (2007).
- 455 2. Agostoni, E., Chinnock, J. E., De Burgh Daly, M. & Murray, J. G. Functional and
456 Histological Studies of the Vagus Nerve and its Branches to the Heart, Lungs and
457 Abdominal Viscera in the Cat. *J. Physiol.* (1957).
- 458 3. Andrews, P. L. R. Vagal afferent innervation of the gastrointestinal tract. *Prog. Brain Res.*
459 **67**, 65–86 (1986).
- 460 4. Berthoud, H. R. & Neuhuber, W. L. Functional and chemical anatomy of the afferent
461 vagal system. *Auton. Neurosci. Basic Clin.* **85**, 1–17 (2000).
- 462 5. Borovikova, L. V *et al.* Vagus nerve stimulation attenuates the systemic inflammatory
463 response to endotoxin. *Nature* **405**, 458–462 (2000).
- 464 6. Browning, K. N., Verheijden, S. & Boeckxstaens, G. E. The Vagus Nerve in Appetite
465 Regulation, Mood, and Intestinal Inflammation. *Gastroenterology* **152**, 730–744 (2017).

- 466 7. Berthoud, H. R. The vagus nerve, food intake and obesity. *Regul. Pept.* **149**, 15–25
467 (2008).
- 468 8. Waise, T. M. Z., Dranse, H. J. & Lam, T. K. T. The metabolic role of vagal afferent
469 innervation. *Nat. Rev. Gastroenterol. Hepatol.* **15**, 625–636 (2018).
- 470 9. Qing, K. Y. *et al.* B fibers are the best predictors of cardiac activity during Vagus nerve
471 stimulation. *Bioelectron. Med.* **4**, 5 (2018).
- 472 10. Kajekar, R., Proud, D., Myers, A. C., Meeker, S. N. & Udem, B. J. Characterization of
473 vagal afferent subtypes stimulated by bradykinin in guinea pig trachea. *J. Pharmacol. Exp.*
474 *Ther.* **289**, 682–687 (1999).
- 475 11. Hoffman, H. H. & Schnitzlein, H. N. The numbers of nerve fibers in the vagus nerve of
476 man. *Anat. Rec.* **139**, 429–435 (1961).
- 477 12. Evans, D. H. L. & Murray, J. G. Histological and Functional Studies on the Fibre
478 Composition of the Vagus Nerve of the Rabbit. *J. Anat.* **88**, 320–37 (1954).
- 479 13. Foley, J. O. & DuBois, F. S. Quantitative Studies of the Vagus Nerve in the Cat. I. The
480 Ratio of Sensory to Motor Fibers. *J. Comp. Neurol.* **67**, (1937).
- 481 14. Tracey, K. J. The Revolutionary Future of Bioelectronic Medicine. *Bioelectron. Med.* **1**,
482 (2014).
- 483 15. Birmingham, K. *et al.* Bioelectronic medicines: A research roadmap. *Nat. Rev. Drug*
484 *Discov.* **13**, 399–400 (2014).
- 485 16. Pavlov, V. A. & Tracey, K. J. Bioelectronic medicine: updates, challenges and paths
486 forward. *Bioelectron. Med.* **5**, 1–4 (2019).
- 487 17. Ben-Menachem, E. Vagus-nerve stimulation for the treatment of epilepsy. *Lancet Neurol.*
488 **1**, 477–482 (2002).
- 489 18. Dawson, J. *et al.* Safety, feasibility, and efficacy of vagus nerve stimulation paired with
490 upper-limb rehabilitation after ischemic stroke. *Stroke* **47**, 143–150 (2016).
- 491 19. Spindler, P., Bohlmann, K., Straub, H. B., Vajkoczy, P. & Schneider, U. C. Effects of
492 vagus nerve stimulation on symptoms of depression in patients with difficult-to-treat
493 epilepsy. *Seizure* **69**, 77–79 (2019).
- 494 20. Koopman, F. A. *et al.* Vagus nerve stimulation inhibits cytokine production and attenuates
495 disease severity in Rheumatoid arthritis. *Proc. Natl. Acad. Sci. U. S. A.* **113**, 8284–8289
496 (2016).
- 497 21. Apovian, C. M. *et al.* Two-Year Outcomes of Vagal Nerve Blocking (vBloc) for the
498 Treatment of Obesity in the ReCharge Trial. *Obes. Surg.* **27**, 169–176 (2017).

- 499 22. Shikora, S. a *et al.* Intermittent Vagal Nerve Block for Improvements in Obesity,
500 Cardiovascular Risk Factors, and Glycemic Control in Patients with Type 2 Diabetes
501 Mellitus: 2-Year Results of the VBLOC DM2 Study. *Obes Surg* (2015)
502 doi:10.1007/s11695-015-1914-1.
- 503 23. McCallum, G. A. *et al.* Chronic interfacing with the autonomic nervous system using
504 carbon nanotube (CNT) yarn electrodes. *Sci. Rep.* **7**, 1–14 (2017).
- 505 24. Yan, D. *et al.* Microneedle Penetrating Array with Axon-Sized Dimensions for Cuff-less
506 Peripheral Nerve Interfacing. *Proc. 9th Int. IEEE EMBS Conf. Neural Eng.* 827–830
507 (2019).
- 508 25. Micera, S. & Navarro, X. Bidirectional Interfaces with the Peripheral Nervous System.
509 *Int. Rev. Neurobiol.* **86**, 23–38 (2009).
- 510 26. Larson, C. E. & Meng, E. A Review for the Peripheral Nerve Interface Designer. *J.*
511 *Neurosci. Methods* **332**, 108523 (2019).
- 512 27. Guo, T. *et al.* Extracellular single-unit recordings from peripheral nerve axons in vitro by
513 a novel multichannel microelectrode array. *Sensors Actuators, B Chem.* **315**, (2020).
- 514 28. Gabella, G. & Pease, H. L. Number of axons in the abdominal vagus of the rat. *Brain Res.*
515 **58**, 465–469 (1973).
- 516 29. Prechtl, J. C. & Powley, T. L. The fiber composition of the abdominal vagus of the rat.
517 *Anat. Embryol. (Berl)*. **181**, 101–115 (1990).
- 518 30. Ward, M. P. *et al.* A flexible platform for biofeedback-driven control and personalization
519 of Electrical nerve stimulation therapy. *IEEE Trans. Neural Syst. Rehabil. Eng.* **23**, 475–
520 484 (2015).
- 521 31. Gillis, W. F. *et al.* Carbon fiber on polyimide ultra-microelectrodes. *J. Neural Eng.* **15**,
522 (2018).
- 523 32. Silverman, H. A. *et al.* Standardization of methods to record Vagus nerve activity in mice.
524 *Bioelectron. Med.* **4**, 1–13 (2018).
- 525 33. Zanos, T. *et al.* Identification of cytokine-specific sensory neural signals by decoding
526 murine vagus nerve activity. *Proc. Natl. Acad. Sci.* in press (2018)
527 doi:10.1073/pnas.1719083115.
- 528 34. Shikano, Y., Nishimura, Y., Okonogi, T., Ikegaya, Y. & Sasaki, T. Vagus nerve spiking
529 activity associated with locomotion and cortical arousal states in a freely moving rat. *Eur.*
530 *J. Neurosci.* **49**, 1298–1312 (2019).
- 531 35. González-González, M. A. *et al.* Thin Film Multi-Electrode Softening Cuffs for Selective
532 Neuromodulation. *Sci. Rep.* **8**, 1–15 (2018).

- 533 36. Masi, E. B. *et al.* Identification of hypoglycemia-specific neural signals by decoding
534 murine vagus nerve activity. *Bioelectron. Med.* **5**, (2019).
- 535 37. Mathews, K. S. *et al.* Acute monitoring of genitourinary function using intrafascicular
536 electrodes: Selective pudendal nerve activity corresponding to bladder filling, bladder
537 fullness, and genital stimulation. *Urology* **84**, 722–729 (2014).
- 538 38. Wark, H. A. C. *et al.* A new high-density (25 electrodes/mm²) penetrating microelectrode
539 array for recording and stimulating sub-millimeter neuroanatomical structures. *J. Neural*
540 *Eng.* **10**, (2013).
- 541 39. DiBona, G. & Sawin, L. Role of Renal Alpha-2-Adrenergic Receptors in Spontaneously
542 Hypertensive Rats. *Hypertension* **9**, (1987).
- 543 40. DiBona, G. F., Sawin, L. L. & Jones, S. Y. Differentiated sympathetic neural control of
544 the kidney. *Am. J. Physiol.* **271**, R84–R90 (1996).
- 545 41. Kozai, T. *et al.* Ultrasmall Implantable Composite Microelectrodes with Bioactive
546 Surfaces for Chronic Neural Interfaces. *Nat. Mater.* **11**, 1065–73 (2012).
- 547 42. Patel, P. R. *et al.* Insertion of linear 8.4 μ m diameter 16 channel carbon fiber electrode
548 arrays for single unit recordings. *J. Neural Eng.* **12**, 046009 (2015).
- 549 43. Patel, P. R. *et al.* Chronic in vivo stability assessment of carbon fiber microelectrode
550 arrays. *J. Neural Eng.* **13**, 066002 (2016).
- 551 44. Welle, E. J. *et al.* Ultra-small carbon fiber electrode recording site optimization and
552 improved in-vivo chronic recording yield. *J. Neural Eng.* (2020).
- 553 45. Moffitt, M. a & McIntyre, C. C. Model-based analysis of cortical recording with silicon
554 microelectrodes. *Clin. Neurophysiol.* **116**, 2240–50 (2005).
- 555 46. Henze, D. A. *et al.* Intracellular features predicted by extracellular recordings in the
556 hippocampus in vivo. *J. Neurophysiol.* **84**, 390–400 (2000).
- 557 47. Rey, H. G., Pedreira, C. & Quian Quiroga, R. Past, present and future of spike sorting
558 techniques. *Brain Res. Bull.* **119**, 106–117 (2015).
- 559 48. Chang, R. B., Strohlic, D. E., Williams, E. K., Umans, B. D. & Liberles, S. D. Vagal
560 sensory neuron subtypes that differentially control breathing. *Cell* **161**, 622–633 (2015).
- 561 49. McAllen, R. M., Shafton, A. D., Bratton, B. O., Trevaks, D. & Furness, J. B. Calibration
562 of thresholds for functional engagement of vagal A, B and C fiber groups in vivo .
563 *Bioelectron. Med.* **1**, 21–27 (2018).
- 564 50. Niijima, A. Glucose-sensitive afferent nerve fibers in the liver and their role in food intake
565 and blood glucose regulation. *J. Auton. Nerv. Syst.* **9**, 207–20 (1983).

- 566 51. Skovsted, P. & Saphthavichaikul, S. The Effects of Isoflurane on Arterial Pressure, Pulse
567 Rate, Autonomic Nervous Activity, and Barostatic Reflexes. *Canad. Anaesth. Soc. J.* **24**,
568 (1977).
- 569 52. Carli, F., Ronzoni, G., Webster, J., Khan, K. & Elia, M. The independent metabolic
570 effects of halothane and isoflurane anaesthesia. *Acta Anaesthesiol. Scand.* **37**, 672–678
571 (1993).
- 572 53. Welle, E. J. *et al.* Fabrication and characterization of a carbon fiber peripheral nerve
573 electrode appropriate for chronic recording. in *Society for Neuroscience 49th Annual*
574 *Meeting, Chicago, IL*, (2019).
- 575 54. Chaure, F. J., Rey, H. G. & Quian Quiroga, R. A novel and fully automatic spike-sorting
576 implementation with variable number of features. *J. Neurophysiol.* **120**, 1859–1871
577 (2018).

578

579

580 **Acknowledgements**

581 We thank Dr. Randy Seeley and Dr. Malcolm Low for their advice on designing the experiments,
582 Dr. Zach Sperry, Aileen Ouyang, Eric Kennedy and Dr. Lauren Zimmerman for their assistance
583 in surgical preparation, Joey Letner for his guidance on data analysis, and Dr. Steve Kemp, Dr.
584 Dan Ursu, Jana Moon, Charles Hwang and Sasha Meshinchi for preparing and imaging the
585 immunohistochemistry nerve sample. This research was supported by the National Institute of
586 Health (NIH) Stimulating Peripheral Activity to Relieve Conditions (SPARC) Program (Award
587 1OT2OD024907) and the National Science Foundation (Award 1707316).

588

589

590

591

592 **Author Contributions**

593 Planned study – AJ, JS, CC, TB. Fabricated arrays – EW, PP, JR, CC. Performed surgeries and
594 collected data – AJ, DR, EB, TB. Analyzed data – AJ, DR, EB, TB. Drafted manuscript – AJ, TB.
595 Reviewed manuscript and approved final version – AJ, DR, EW, PP, JR, EB, JS, CC, TB.

596

597 **Competing Interests**

598 Authors CAC, EJW, JPS, PRP, AAJ, and TMB are co-authors on a patent application on the
599 development of the carbon fiber microelectrode array. Priority date June 22, 2018. Application #
600 PCT/US2019/038500. The authors declare no other competing interests.

601

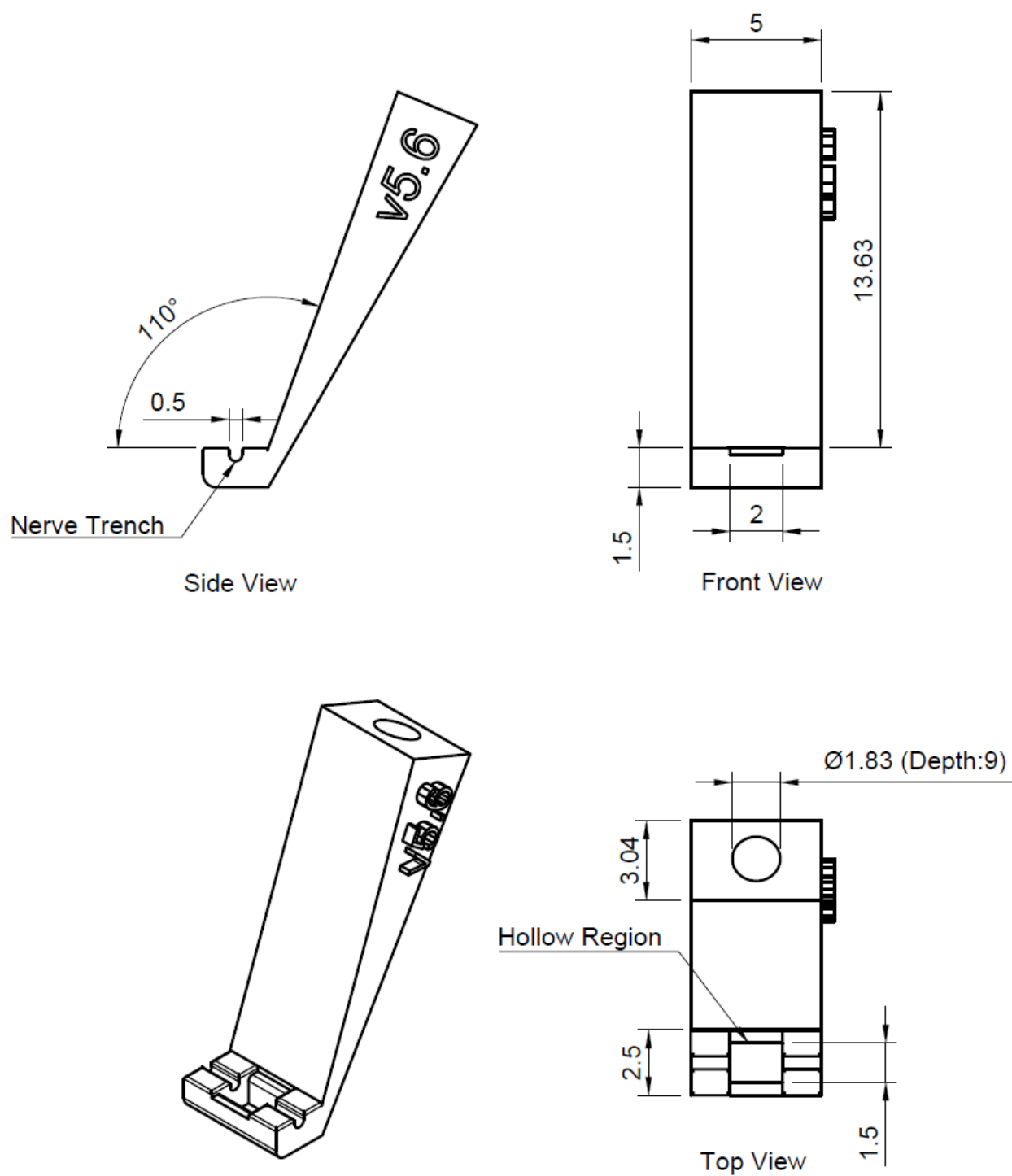
602

603 **Supplementary Information**

604 **Supplementary Table 1. Summary for all the experiments with inserted CFMA in the vagus nerve.**

ID	IP Dose	Array	Functional CF	CF with Activity	Clusters	Vpp (μV)	SNR	Clusters with $ \rho \geq 0.3$			Signal Propagation (m/sec)		
								BG	BR	HR	Afferent	Efferent	Max Span (μm)
1	Glucose	A	16	16	16	21.8 - 27.5	2.4 - 3.1	0	0	0	-	-	-
2	2-DG	A	16	6	6	18.7 - 34.5	2.3 - 3.5	6	6	3	-	-	-
3	Glucose	A	15	5	5	17.9 - 29.2	2.0 - 3.0	3	2	1	-	-	-
4	Insulin	A	15	14	15	23.2 - 91.7	2.5 - 8.3	14	15	15	0.7	0.7	396
5	Saline	A	15	7	8	22.0 - 43.9	2.5 - 3.5	7	7	6	0.7	0.7	264
6	Insulin	A	14	0	0	-	-	-	-	-	-	-	-
7	Glucose	B	16	0	0	-	-	-	-	-	-	-	-
8	Insulin	C	16	7	8	20.4 - 40.5	2.9 - 5.3	8	8	8	-	-	-
9	Saline	C	16	6	7	20.7 - 59.1	3.3 - 7.2	2	2	5	-	0.7	132
10	2-DG	C	16	16	16	21.1 - 58.7	3.0 - 6.9	13	11	14	0.7	0.7 - 8.8	528
11	Glucose	D	16	6	6	15.1 - 38.4	2.8 - 4.6	6	6	5	0.7	-	132
12	Insulin	E	14	5	6	17.7 - 78.2	2.8 - 7.9	2	6	5	-	-	-
13	2-DG	C	14	2	2	27.5 - 44.0	3.6 - 5.7	2	2	2	-	-	-
14	Saline	A	14	14	14	27.4 - 62.8	2.7 - 5.5	13	14	14	0.7-0.9	-	792
15	Insulin	D	16	14	16	18.7 - 54.3	2.4 - 6.5	11	11	12	0.7	-	660
16	2-DG	D	16	13	13	17.3 - 35.6	2.4 - 4.0	11	9	4	0.7	-	792
17	Insulin	D	16	14	14	20.0 - 26.6	2.8 - 3.5	11	12	11	0.7-1.0	-	528
18	Glucose	D	15	2	2	18.8 - 26.0	3.1 - 3.2	2	0	2	0.7	-	132
19	2-DG	D	15	4	4	19.3 - 36.5	3.1 - 4.7	4	4	4	-	-	-
20	Saline	F	8	0	0	-	-	-	-	-	-	-	-
21	Glucose	A	12	1	1	26.7	2.8	1	1	1	-	-	-
22	2-DG	D	15	15	15	27.5 - 54.0	3.1 - 6.4	8	10	11	0.7 - 0.9	0.7	528
Total			326	167	174	15.1 - 91.7	2.0 - 8.3	124	126	123	0.7-1.0	0.7 - 8.8	132 - 792

605 Correlation coefficients (ρ) were calculated between cluster firing rates and blood glucose (BG) concentrations,
 606 breathing rate (BR) and heart rate (HR) measurements.



607

608

609 **Supplementary Figure 1. Nerve-holder design for inserting CFMA in a rat cervical vagus nerve. Dimensions**
610 **are in millimeters (mm).**

611